WILEY-VCH

Edited by Markus Antonietti and Klaus Müllen

Chemical Synthesis and Applications of Graphene and Carbon Materials

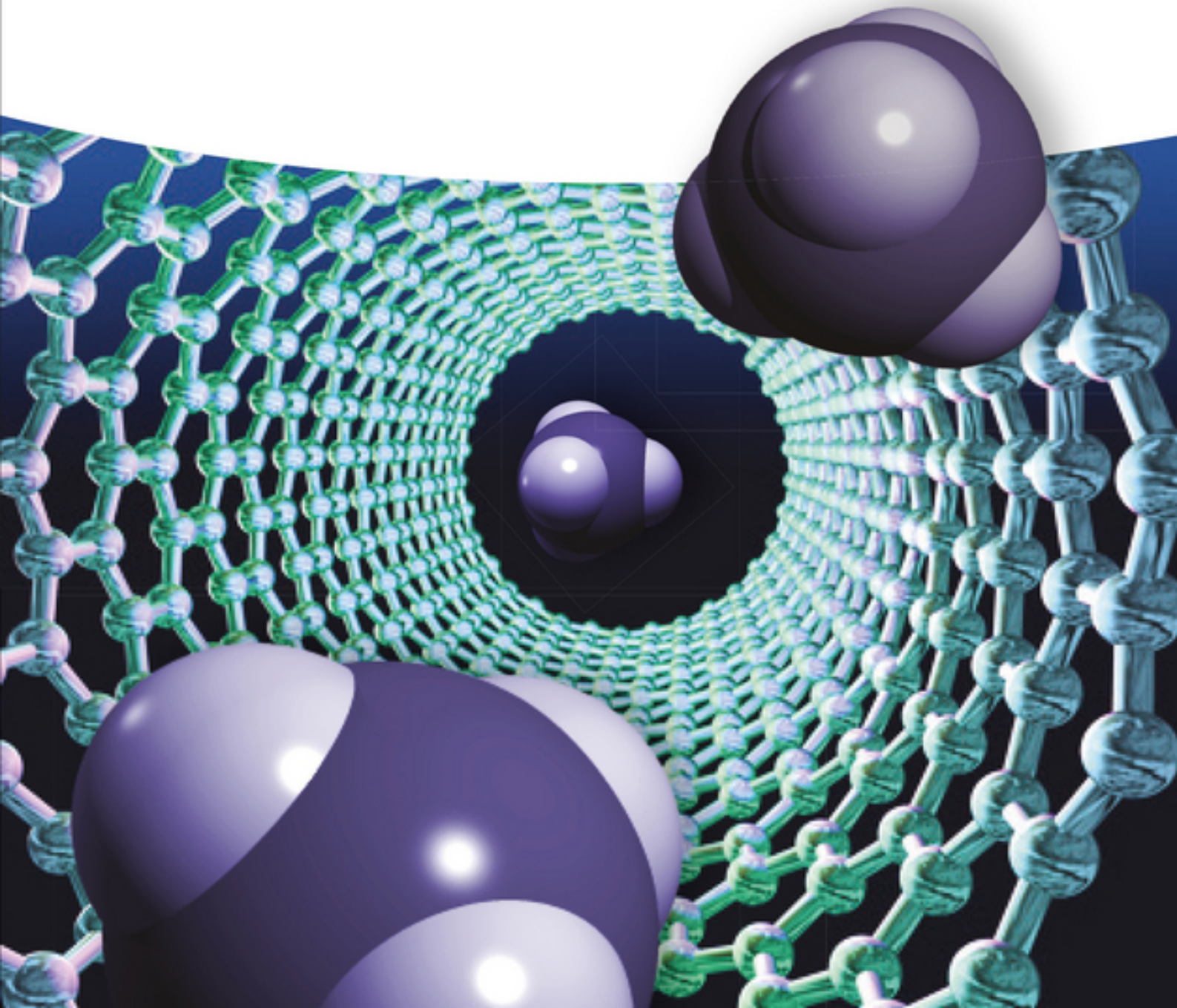

Chemical Synthesis and Applications of Graphene and Carbon Materials

Chemical Synthesis and Applications of Graphene and Carbon Materials

Edited by Markus Antonietti and Klaus Müllen

WILEY-VCH
Verlag GmbH & Co. KGaA

The Editors

Prof. Markus Antonietti
MPI of Colloids and Interfaces
Colloid Chemistry
Research Campus Golm
Colloid Chemistry
14424 Potsdam
Germany

Prof. Klaus Müllen
MPI für Polymerforschung
Ackermannweg 10
55128 Mainz
Germany

Cover
Promotive/Shutterstock

Library of Congress Card No.: applied for

British Library Cataloguing-in-Publication Data
A catalogue record for this book is available from the British Library.

Bibliographic information published by the Deutsche Nationalbibliothek
The Deutsche Nationalbibliothek lists this publication in the Deutsche Nationalbibliografie; detailed bibliographic data are available on the Internet at http://dnb.d-nb.de.

Print ISBN: 978-3-527-33208-3
ePDF ISBN: 978-3-527-64819-1
ePub ISBN: 978-3-527-64818-4
Mobi ISBN: 978-3-527-64817-7
oBook ISBN: 978-3-527-64816-0

Typesetting SPi Global, Chennai, India
Printing and Binding

Printed on acid-free paper

Contents

List of Contributors

Yas Fadel Al-Hadeethi
King Abdulaziz University
Department of Physics
Jeddah 21589
Kingdom of Saudi Arabia

Elena Bekyarova
University of California—Riverside
Center for Nanoscale Science and Engineering
104 Pierce Hall Annex
Riverside, CA 92521
USA

Yongsheng Chen
Nankai University
Department of Chemistry
Institute of Polymer Chemistry
Key Laboratory of Functional Polymer Materials
Center for Nanoscale Science and Technology, 94, Weijin Road
Nankai District, Tianjin 300071
China

Basant Chitara
Indian Institute of Science
Materials Research Centre
Bangalore 560012
India

Barun Das
Chemistry and Physics of Materials Unit
New Chemistry Unit
International Centre for Materials Science, CSIR Centre of Excellence in Chemistry and Sheik Saqr Laboratory
Jawaharlal Nehru Centre for Advanced Scientific Research
Jakkur, Bangalore 560064
India

K. Gopalakrishnan
Chemistry and Physics of Materials Unit
New Chemistry Unit
International Centre for Materials Science, CSIR Centre of Excellence in Chemistry and Sheik Saqr Laboratory
Jawaharlal Nehru Centre for Advanced Scientific Research
Jakkur, Bangalore 560064
India

Fei Guo
Brown University
School of Engineering and Institute for Molecular and Nanoscale Innovation (IMNI)
182 Hope Street
Providence, RI 02912
USA

Robert C. Haddon
University of California—Riverside
Center for Nanoscale Science and Engineering
104 Pierce Hall Annex
Riverside, CA 92521
USA

University of California—Riverside
Department of Chemistry
104 Pierce Hall Annex
Riverside, CA 92521
USA

King Abdulaziz University
Department of Physics
Jeddah 21589
Kingdom of Saudi Arabia

University of California—Riverside
Department of Chemical and Environmental Engineering
104 Pierce Hall Annex
Riverside, CA 92521
USA

Guang-Ping Hao
School of Chemical Engineering
Faculty of Chemical, Environmental and Biological Science and Technology
State Key Laboratory of Fine Chemicals
Dalian University of Technology
Linggong Road 2, Ganjingzi District
Dalian 116024
PR China

Mark C. Hersam
Northwestern University
Department of Materials Science and Engineering
2220 Campus Drive
Evanston, IL 60208
USA

Northwestern University
Departments of Chemistry and Medicine
2220 Campus Drive
Evanston, IL 60208
USA

Andreas Hirsch
University of Erlangen-Nuremberg
Department of Chemistry and Pharmacy
Henkestrasse 42, 91054 Erlangen
Germany

Lu Huang
Nankai University
Department of Chemistry
Institute of Polymer Chemistry
Key Laboratory of Functional Polymer Materials
Center for Nanoscale Science and Technology, 94, Weijin Road
Nankai District, Tianjin 300071
China

Yi Huang
Nankai University
Department of Chemistry
Institute of Polymer Chemistry
Key Laboratory of Functional Polymer Materials
Center for Nanoscale Science and Technology, 94, Weijin Road
Nankai District, Tianjin 300071
China

Robert Hurt
Brown University
School of Engineering and Institute for Molecular and Nanoscale Innovation (IMNI)
182 Hope Street
Providence, RI 02912
USA

Mikhail E. Itkis
University of California—Riverside
Center for Nanoscale Science and Engineering
104 Pierce Hall Annex
Riverside, CA 92521
USA

University of California—Riverside
Department of Chemistry
104 Pierce Hall Annex
Riverside, CA 92521
USA

Mietek Jaroniec
Kent State University
Department of Chemistry and Biochemistry
214 Williams Hall
Kent, OH 44242
USA

Neetu Jha
University of California—Riverside
Center for Nanoscale Science and Engineering
104 Pierce Hall Annex
Riverside, CA 92521
USA

University of California—Riverside
Department of Chemistry
104 Pierce Hall Annex
Riverside, CA 92521
USA

Irina Kalinina
University of California—Riverside
Center for Nanoscale Science and Engineering
104 Pierce Hall Annex
Riverside, CA 92521
USA

University of California—Riverside
Department of Chemistry
104 Pierce Hall Annex
Riverside, CA 92521
USA

University of California—Riverside
Department of Chemistry
104 Pierce Hall Annex
Riverside, CA 92521
USA

Eun Kyung Kim
Carnegie Mellon University
Department of Chemical and Environmental Engineering
P.O. Box 208286
New Haven, CT 06520
USA

Tomasz Kowalewski
Carnegie Mellon University
Department of Chemical and Environmental Engineering
P.O. Box 208286
New Haven, CT 06520
USA

S. B. Krupanidhi
Indian Institute of Science
Materials Research Centre
Bangalore 560012
India

Prashant Kumar
Chemistry and Physics of Materials Unit
New Chemistry Unit
International Centre for Materials Science, CSIR Centre of Excellence in Chemistry and Sheik Saqr Laboratory
Jawaharlal Nehru Centre for Advanced Scientific Research
Jakkur, Bangalore 560064
India

Wen-Cui Li
School of Chemical Engineering
Faculty of Chemical, Environmental and Biological Science and Technology
State Key Laboratory of Fine Chemicals
Dalian University of Technology
Linggong Road 2, Ganjingzi District
Dalian 116024
PR China

Xianglong Li
National Center for Nanoscience and Technology
No. 11 Zhongguancun Beiyitiao
Zhongguancun, Beijing 100190
China

Yu Teng Liang
Northwestern University
Department of Materials Science and Engineering
2220 Campus Drive
Evanston, IL 60208
USA

An-Hui Lu
School of Chemical Engineering
Faculty of Chemical, Environmental and Biological Science and Technology
State Key Laboratory of Fine Chemicals
Dalian University of Technology
Linggong Road 2, Ganjingzi District
Dalian 116024
PR China

Bin Luo
National Center for Nanoscience and Technology
No. 11 Zhongguancun Beiyitiao
Zhongguancun, Beijing 100190
China

Urmimala Maitra
Chemistry and Physics of Materials Unit
New Chemistry Unit
International Centre for Materials Science, CSIR Centre of Excellence in Chemistry and Sheik Saqr Laboratory
Jawaharlal Nehru Centre for Advanced Scientific Research
Jakkur, Bangalore 560064
India

H.S.S. Ramakrishna Matte
Chemistry and Physics of Materials Unit
New Chemistry Unit
International Centre for Materials Science, CSIR Centre of Excellence in Chemistry and Sheik Saqr Laboratory
Jawaharlal Nehru Centre for Advanced Scientific Research
Jakkur, Bangalore 560064
India

Krzysztof Matyjaszewski
Carnegie Mellon University
Department of Chemical and Environmental Engineering
P.O. Box 208286
New Haven, CT 06520
USA

John P. McGann
Carnegie Mellon University
Department of Chemical and Environmental Engineering
P.O. Box 208286
New Haven, CT 06520
USA

Sittichai Natesakhawat
United States Department of Energy
National Energy Technology Laboratory
P.O. Box 10940
Pittsburgh, PA 15236
USA

Sandip Niyogi
University of California—Riverside
Center for Nanoscale Science and Engineering
104 Pierce Hall Annex
Riverside, CA 92521
USA

University of California—Riverside
Department of Chemistry
104 Pierce Hall Annex
Riverside, CA 92521
USA

Jens Peter Paraknowitsch
Technische Universität Berlin
Department of Chemistry Functional Materials
Hardenbergstr. 40, 10623 Berlin
Germany

C. N. R. Rao
Chemistry and Physics of Materials Unit
New Chemistry Unit
International Centre for Materials Science, CSIR Centre of Excellence in Chemistry and Sheik Saqr Laboratory
Jawaharlal Nehru Centre for Advanced Scientific Research
Jakkur, Bangalore 560064
India

Indian Institute of Science
Materials Research Centre
Bangalore 560012
India

Santanu Sarkar
University of California—Riverside
Center for Nanoscale Science and Engineering
104 Pierce Hall Annex
Riverside, CA 92521
USA

University of California—Riverside
Department of Chemistry
104 Pierce Hall Annex
Riverside, CA 92521
USA

K. S. Subrahmanyam
Chemistry and Physics of Materials Unit
New Chemistry Unit
International Centre for Materials Science, CSIR Centre of Excellence in Chemistry and Sheik Saqr Laboratory
Jawaharlal Nehru Centre for Advanced Scientific Research
Jakkur, Bangalore 560064
India

Qiang Sun
School of Chemical Engineering
Faculty of Chemical, Environmental and Biological Science and Technology
State Key Laboratory of Fine Chemicals
Dalian University of Technology
Linggong Road 2, Ganjingzi District
Dalian 116024
PR China

Arne Thomas
Technische Universität Berlin
Department of Chemistry
Functional Materials
Hardenbergstr. 40, 10623 Berlin
Germany

Max von Delius
University of Ulm
Institute of Organic Chemistry and Advanced Materials
Albert-Einstein-Allee 11
89081 Ulm
Germany

Bin Wang
National Center for Nanoscience and Technology
No. 11 Zhongguancun Beiyitiao
Zhongguancun, Beijing 100190
China

Qingxiao Wang
King Abdullah University of Science and Technology
Advanced Nanofabrication, Imaging and Characterization Core Lab
Thuwal 23955
Kingdom of Saudi Arabia

Jay F. Whitacre
Carnegie Mellon University
Department of Material Science and Engineering
5000 Forbes Avenue
Pittsburgh, PA 15213
USA

Yanfei Xu
Nankai University
Department of Chemistry
Institute of Polymer Chemistry
Key Laboratory of Functional Polymer Materials
Center for Nanoscale Science and Technology, 94, Weijin Road
Nankai District, Tianjin 300071
China

Weibo Yan
Nankai University
Department of Chemistry
Institute of Polymer Chemistry
Key Laboratory of Functional Polymer Materials
Center for Nanoscale Science and Technology, 94, Weijin Road
Nankai District, Tianjin 300071
China

Xiang-Qian Zhang
School of Chemical Engineering
Faculty of Chemical, Environmental and Biological Science and Technology
State Key Laboratory of Fine Chemicals
Dalian University of Technology
Linggong Road 2, Ganjingzi District
Dalian 116024
PR China

Xixiang Zhang
King Abdullah University of Science and Technology
Advanced Nanofabrication, Imaging and Characterization Core Lab
Thuwal 23955
Kingdom of Saudi Arabia

Linjie Zhi
National Center for Nanoscience and Technology
No. 11 Zhongguancun Beiyitiao
Zhongguancun, Beijing 100190
China

Mingjiang Zhong
Carnegie Mellon University
Department of Chemical and Environmental Engineering
P.O. Box 208286
New Haven, CT 06520
USA

Yale University
Department of Chemical and Environmental Engineering
P.O. Box 208286
New Haven, CT 06520
USA

1

Block Copolymer Templating as a Path to Porous Nanostructured Carbons with Highly Accessible Nitrogens for Enhanced (Electro)chemical Performance[1]

John P. McGann, Mingjiang Zhong, Eun Kyung Kim, Sittichai Natesakhawat, Mietek Jaroniec, Jay F. Whitacre, Krzysztof Matyjaszewski, and Tomasz Kowalewski

1.1 Introduction

Historically, graphitic and semi-graphitic materials have always played a major role in a wide range of electrical and electrochemical systems. The past two decades have brought some of the most interesting synthetic and processing advances in the area of advanced carbon materials, including the discovery and/or isolation of several sp^2 allotropes (fullerenes, carbon nanotubes, graphene, etc.). In addition, a variety of top-down [1–3] and bottom-up [4] synthetic approaches emerged as a way to control the architecture and chemical functionality.

This, in turn, has led to the development of nanostructured carbons for advanced applications such as supercapacitors, fuel cells, batteries, water-splitting systems, sensors, and gas chemisorbents [5, 6].

In the past, the focus of the field of advanced carbons has been gradually shifting from control over the nanostructure to control over the chemical functionality. One of the most important driving forces in the quest for such "chemical nanocarbons" has been the growing understanding of the electronic properties of graphene. The next breakthroughs in this area can be expected to involve more precise control of the edge states of graphenic domains, including the incorporation of heteroatoms and more complex functionalities [5, 7]. Nitrogen is a particularly attractive heteroatom because of its relative ease of incorporation and abundance in various carbon precursors. Viewed simplistically, nitrogen doping (N-doping) introduces basicity into the carbon structure that can be utilized for a variety of electrochemical and electrocatalytic systems; however, the detailed chemistry behind its effect is still poorly understood. This is largely due to the complexities arising from the heterogeneous nature and, still, relatively ill-defined structure of many of the materials studied. As shown in Figure 1.1, the edge functionalities can be introduced in graphene either through the attachment of pendant groups (e.g., amine, Figure 1.1a) or through edge substitution with heteroatoms (Figure 1.1b,c). Basal plane substitution (quaternary nitrogen, Figure 1.1d) should not significantly impart electrochemical properties [5].

Pyridinic nitrogens (Figure 1.1b) incorporated into the graphitic network are often thought to be the most reactive and beneficial nitrogen-containing functionality for

[1] [8], Reproduced with permission of Wiley.

Chemical Synthesis and Applications of Graphene and Carbon Materials, First Edition.
Edited by Markus Antonietti and Klaus Müllen.

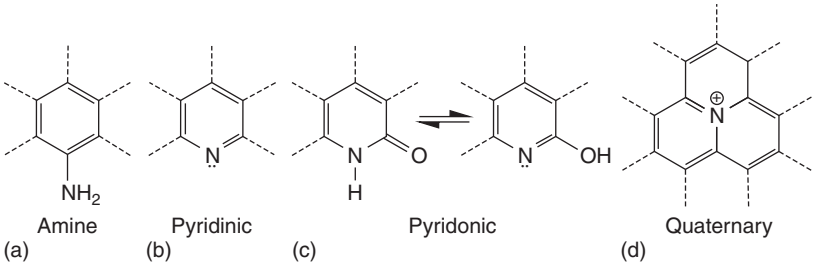

Figure 1.1 Common N-functionalities in graphitic systems. ([8], Reproduced with permission of Wiley.)

electrochemical systems [5]. While there are many synthetic routes to N-doped carbon materials, two key requirements are necessary to fully realize the advantages afforded through graphitic edge N-doping: (i) efficient formation of pyridinic species and (ii) assurance of their (electro)chemical accessibility. The latter could be accomplished by designing material with high-surface area nanoporous structure with pyridinic species preferentially exposed on pore wall surfaces.

In this chapter, we demonstrate how these two requirements can be satisfied simultaneously through the general approach developed in recent years in our laboratories, in which the nanostructure of carbon is templated by the self-assembly of block copolymer or hybrid precursors comprised of a carbon source and a sacrificial block/element [9–23]. In these materials, which will be referred to as copolymer templated nitrogen-rich carbons (CTNCs), high nitrogen content polyacrylonitrile (PAN) is the carbon precursor of choice since its carbonization results in high content of pyridinic functionalities [24]. For block copolymer templating, the sacrificial block needs to be immiscible with the carbon source to assure nanoscale phase separation and formation of well-defined template morphology. Heat treatment results in an N-doped carbon material with morphology replicating the copolymer precursor [9, 11, 13]. As discussed below, copolymer templates of certain compositions afford materials with high surface area and efficient nitrogen exposure to the pore walls, presumably through preferential orientation of PAN chains at the interface with the sacrificial block.

Following a more detailed discussion on the motivation for this choice of templating approach when compared with other methods, this chapter will discuss the structural aspects CTNCs and their performance in applications such as supercapacitors, oxygen-reduction reactions (ORRs), and CO_2 adsorption. Since the main goal of this contribution is to discuss the merits of CTNCs with respect to other approaches in the synthesis of nitrogen-rich electroactive carbons, a particularly strong emphasis will be placed on the critical overview of the other strategies.

1.2 Electronic Properties of Graphene Edges

The electronic structure of nanographenes is predominantly controlled by quantum confinement effects [25] and edge effects [26–30], with the latter providing particular opportunities for chemical tunability. It has been shown computationally

that when graphene is spatially confined to the nanometer scale in two dimensions (nanographene), a density of states (DOS) arises at the Fermi level [27, 31–33]. These states (HOMO/LUMO) are non-bonding and are predominantly localized at the zigzag edges. Their existence has been subsequently confirmed using scanning tunneling spectroscopy [34, 35] and EPR [36, 37]. The nonbonding character of zigzag edge states leads to unconventional magnetic properties [38] and can be a source of enhanced (electro)chemical activity [5, 39]. In particular, the high electron density of the HOMO along the zigzag edges and their high polarizability make them susceptible to oxidation or other functionalizations [29, 40–42].

So far, electronic calculations for edge-substituted nanographenes have been primarily focused on the π-electron system. For nitrogen substitution, the primary conclusions were that the edge location is the most stable one [43] and that edge nitrogen p_z electrons would also have nonbonding character, with the Fermi level shifted accordingly to the higher electronegativity of nitrogen sites [43–45]. It is also recognized that electronic communication between a lone pair of pyridinic species and a π-electron system should lead to high (electro)chemical activity, desirable in many applications [46].

1.3 Edge Functionalization of Graphene

The strategies for inclusion of nitrogen functionalities at graphene edges can be divided into two groups: (i) a post-pyrolysis procedure via reaction of the carbon material with N-containing gases [44, 47–49] and (ii) carbonization of N-rich precursors [50–58]. Below we briefly discuss the extent to which these approaches address the challenges associated with the control over the location and nature of the N-functionalities in carbon material and with assuring their electrochemical availability.

1.3.1 Post-Pyrolysis Nitrogen Doping

The most common form of post-pyrolysis N-doping is through reaction of the carbon material with ammonia at high temperatures [44, 47, 59–61]. The advantage of this approach is its simplicity and avoidance of any oxygen-containing reactants. However, the corrosive nature of ammonia prevents its use in conventional templating methods using silica or zeolites. Chemical vapor deposition used to incorporate nitrogen into the graphitic lattice introduces primarily quaternary nitrogens [49, 62] while "softer" techniques have been shown to preferentially functionalize the edges and defect sites [44, 45, 63]. One of such "soft" (i.e., low temperature) and versatile approaches to post-pyrolysis edge chemistry involves the selective introduction of azides onto graphene edges through reaction with iodine azide [64] followed by click chemistry [65]. The diversity of alkynes that are commensurable with click chemistry makes this approach particularly promising for the future of tunable carbon materials.

1.3.2 Pyrolysis of Nitrogen-Containing Precursors

An alternative approach to N-rich graphitic material is through the pyrolysis of N-containing precursors. The most common precursor materials used to this end are melamine [54], vinylpyridine resin [66], urea [67], silk fibroin [68], and PAN [9–11, 13, 14, 53, 58, 69–77], some of which offer little N-functionality specificity. An

example of molecularly precise placement of nitrogen on the edges of nanographene involves the use of a bottom-up synthetic approach based on a cyclodehydrogenation of branched oligophenylenes [4], which allows for the exact control of shape (including armchair vs zigzag edges [78]), size [79], and functionality. Incorporation of nitrogen can be accomplished here in a straightforward manner by replacement of some of the phenylenes with nitrogen heterocycles, for example, pyrimidines [80]. Activity of such introduced edge nitrogens has been confirmed by demonstrating their ability to complex Pd(II) and Ru(II) metal salts [80].

Another example of molecularly precise nitrogen-rich carbon is graphitic carbon nitride (g-C_3N_4), usually consisting of tri-connected triazine units, which also represents the upper limit of nitrogen doping in sp^2 hybridized systems. Despite the fact that its polymeric derivative is one of the oldest reported synthetic polymers [81] and that there are many synthetic approaches [82–84], this well-defined semiconductor has only recently found use as a metal-free catalyst in electrochemical reactions [84–91]. One particularly intriguing aspect of g-C_3N_4 is that its molecular framework contains multiple sites that can be utilized for different catalytic functions [84] and can be manipulated to tune the electronic properties [92]. Moreover, it is highly amenable to further modification, for example, through the incorporation of other heteroatoms such as boron and phosphorus [93–96].

1.3.2.1 Polyacrylonitrile

The previous two examples illustrated how the structure of N-doped nanographene can be controlled by the molecular structure of the carbon precursor. Another example of a system that relies on (partial) retention of the elements of molecular architecture is PAN, one of the most commonly used precursors for the production of carbon fibers [58, 97, 98]. The key requirement for carbon precursors used for this purpose is their ability to exhibit a high degree of molecular orientation and to translate it upon carbonization into the orientation of partially graphitic domains. As shown in Scheme 1.1, with PAN this retention is achieved through the stabilization, which involves heat treatment in air between 200 and 300 °C resulting in cyclization of the nitrile groups and formation of

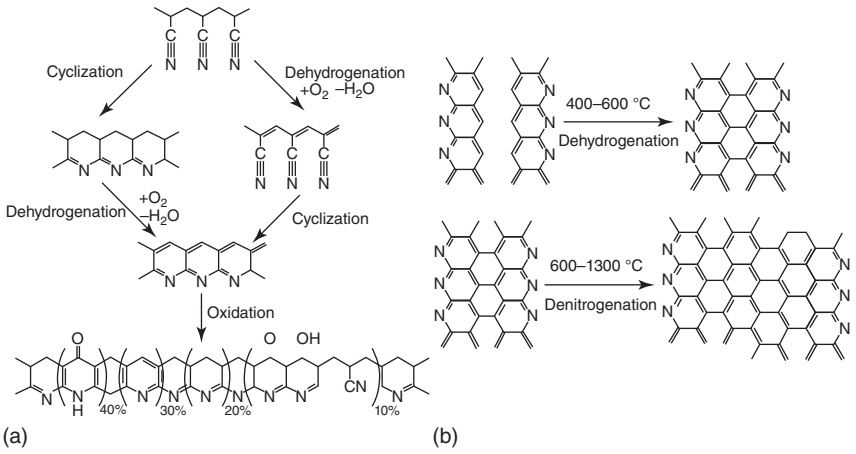

Scheme 1.1 Accepted mechanisms of PAN stabilization (a) and carbonization (b) [24].

a cross-linked ladder polymer primarily consisting of adjacent pyridines and pyridones [24]. Following this step, carbonization is carried out by pyrolysis under inert atmosphere, and proceeds by dehydrogenation (400–600 °C) followed by denitrogenation (>600 °C) [24].

The unique aspect of carbon from PAN is the location of the remaining nitrogens inferred primarily from X-ray photoelectron spectroscopy (XPS) studies of the evolution of nitrogen functionalities upon heat treatment. At lower carbonization temperatures (600–800 °C), pyridinic and pyridonic species (Scheme 1.1) represent the majority of the nitrogen functionalities (70–80%). Further heat treatment (>900 °C) introduces a small component of nitrogens into the basal plane of the nanographenes in a quaternary state. In recent years, high pyridinic nitrogen content in carbons obtained from PAN placed them in the center of the field of N-doped carbons [9, 10, 13, 16–18, 53, 58, 73, 99–102]. Assuring the (electro)chemical availability of nitrogen species remains, however, a major challenge with these materials.

1.4 Block Copolymer Templating as a Path to High Surface Area N-Doped Carbons with Accessible Nitrogen-Containing Graphitic Edges

As discussed above, control over the nanostructure and the molecular orientation is necessary to maximize the impact of the N-edge functionalities. The control of nanostructure is primarily required to assure high surface area of the material, which is the prerequisite of accessibility of N-edge functionalities. Ultimately, however, their wide electrochemical availability necessitates some level of control over the molecular orientation of nanographitic domains with respect to pore walls.

A common path to introducing porosity and to simultaneously control the pore size distribution is through a templating approach, where a well-defined scaffolding material is impregnated with the carbon precursor. The choice of template varies depending mainly on the size of the nanostructure desired. Porous carbon materials containing micropores (pores < 2 nm), mesopores (2–50 nm), and macropores (>50 nm) have been repeatedly demonstrated. The templates are mostly comprised of inorganics such as zeolites [103–107] or silica [11, 17, 20, 76, 108–111], and are removed after carbonization, for example, by acid wash. This approach, however, does not offer much control over the orientation of nanographenes within carbon domains.

An example of the process that allows control over the graphitic orientation is formation of carbon fibers from high carbon yield precursors such as PAN [99, 112] and mesophase-pitch [113]. In such systems graphitic planes typically adopt axial orientation, with possible additional degrees of order (e.g., radial arrangement for mesophase pitch-derived fibers [114]). Although such orientation may result in some exposure of nanographene edges on the surface of the fiber, with the typical fiber dimensions in the range of hundreds of nanometers to several microns, most of the edges remain buried within the bulk of the material. In the remainder of this section, we describe how this dilemma can be solved by simultaneous introduction of porosity and local PAN orientation through the use of block copolymer templating.

The majority of templated synthesis of nanoporous carbons is based on inorganic templates, and relatively limited efforts have been dedicated to soft (organic–organic)

templating [9, 10, 13, 14, 16, 115, 116]. Templating using block copolymers containing PAN and an immiscible sacrificial block (primarily poly(*n*-butyl acrylate) – PBA) has been pioneered in the past decade in our laboratories, with major stimulation coming from the advances in the field of controlled radical polymerization, especially atom transfer radical polymerization [117–128], which opened the way to new and versatile methods for the synthesis of polymers of various architectures (blocks, stars, brushes, etc.) [117–121, 129–133].

The turning point in the development of this route has been the finding that once PAN-*b*-PBA copolymers develop well-defined nanostructures driven by the immiscibility of the blocks, the PAN phase can be thermally stabilized, just as in the process used in the formation of carbon fibers [9]. The degree of stabilization achieved in this way has been shown to be sufficient to facilitate the preservation of the nanostructure upon pyrolysis under inert atmosphere, with PAN domains converting into carbonaceous semi-graphitic phase and the sacrificial block volatilizing, leading to the formation of nanoporous structure (Figure 1.2). The scheme shown in Figure 1.2 points to an additional important aspect of carbonization of PAN-*b*-PBA copolymers: given their partial crystallinity [134–136], PAN domains can form two types of interfaces with the sacrificial block: (i) the covalently bonded interface, perpendicular to the direction of polymer chains and (ii) the non-bonded interface, comprised of the side boundaries of PAN crystallites. Given that, in analogy with carbon fibers, partial graphitization of thermally stabilized PAN domains can be expected to proceed along the polymer chains, this kind of interfacial anisotropy should be retained in the carbonized material. The main consequence of such anisotropy would be the preferential exposure of nitrogen-rich zigzag edges on pore walls originating from the non-bonded interface. Understandably, within such picture, the ultimate fraction of nitrogen-rich edges exposed on pore walls would strongly depend on the polymer morphology, with the minimal exposure expected for lamellar structures, for which the interface with the sacrificial block would be of primarily covalently bonded nature.

While the presented view of molecular orientation effects in PAN-*b*-PBA copolymers and the resultant CNTCs is somewhat simplistic, it is supported by the structural

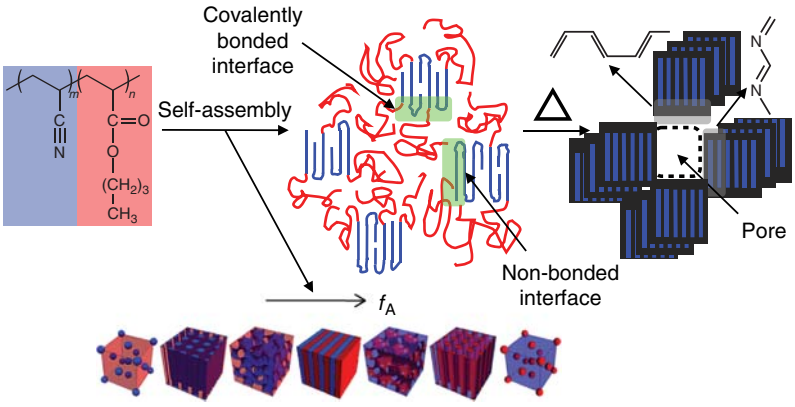

Figure 1.2 Nanometer-scale self-assembly and conversion of PAN-*b*-PBA to a nanoporous N-rich carbon material. The green shaded regions point to the two different types interfaces between the semicrystalline PAN and sacrificial block. ([8], Reproduced with permission of Wiley.)

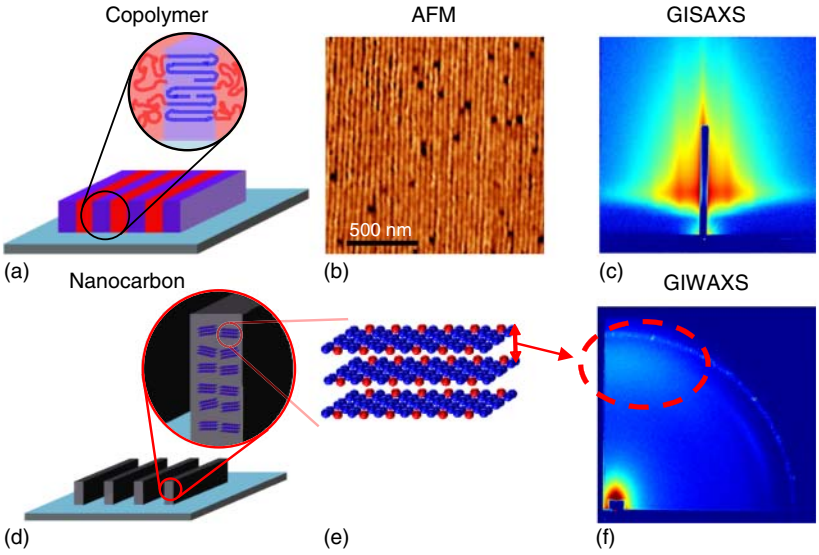

Figure 1.3 (a) Schematic, (b) AFM, and (c) grazing incidence small angle X-ray scattering (GISAXS) of a zone cast thin film of PBA-*b*-PAN and the (d) schematic, (e) comprising stacked nanographenes, and (f) grazing incidence wide angle X-ray scattering (GIWAXS) of the resultant lamellae CTNC film. ([8], Reproduced with permission of Wiley.)

analysis of highly ordered CNTCs obtained from ordered thin films of lamellar PAN-*b*-PBA copolymers prepared by zone casting [13, 137]. Atomic force microscopy (AFM) and grazing incidence small angle X-ray scattering (GISAXS) analysis of zone cast copolymer films (Figure 1.3a–c) and nanocarbons (not shown) revealed the presence of extended, parallel, narrow lamellae perpendicular to the substrate [13, 137]. As illustrated schematically in Figure 1.3a, for a copolymer this kind of structure implies the orientation of PAN chains parallel to the substrate. Analogous anisotropy and in-plane orientation of nanographitic domains in nanocarbon prepared from such ordered copolymer films was evident from the out-of plane position of the broad $\pi-\pi$ stacking (002) peak in grazing incidence wide angle X-ray scattering (GIWAXS) patterns of nanocarbon (Figure 1.3f).

The high degree of preservation of the lamellar nanostructure upon carbonization shown in the last example was facilitated by the presence of the supporting substrate. In the bulk, most morphologies, with the exception of some branching bicontinuous structures, after removal of the sacrificial block typically lead to various degrees of collapse of the three-dimensional nanostructure. The range of copolymer compositions assuring the preservation of nanoscale morphology in the bulk through the presence of contiguous PAN framework has been identified only recently. Small angle X-ray scattering (SAXS) patterns for the copolymer and nanocarbon show evidence of such preservation (Figure 1.4a). The high degree of nanostructure preservation upon carbonization of copolymers within this composition range has been confirmed through detailed analysis of SAXS patterns and nitrogen sorption isotherms.

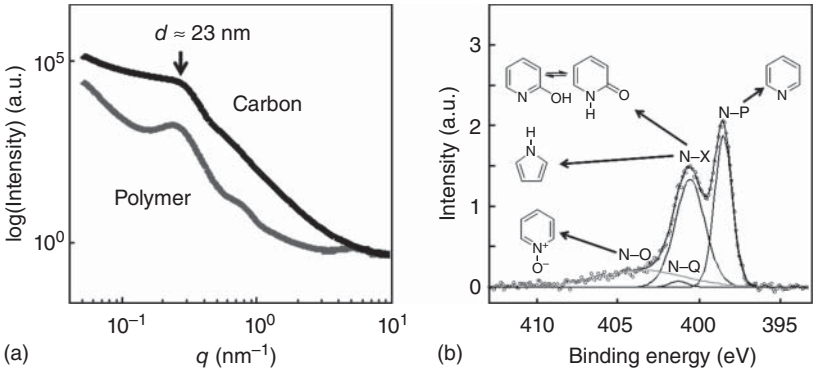

Figure 1.4 (a) Small angle X-ray scattering profiles of AN_{99}-*b*-BA_{70} annealed at 200 °C (dashed) and its corresponding CTNC pyrolyzed at 700 °C (solid). (b) XPS high resolution N 1s spectra of mesoporous carbon prepared from AN_{99}-*b*-BA_{70}. ([8], Reproduced with permission of Wiley.)

One of the particularly interesting structural insights into the environment of pyridinic nitrogens in such prepared materials came from the shape of their N 1s XPS spectral peak, in which the pyridinic peaks were particularly well resolved, with the full width at half maximum (FWHM) after deconvolution equal to about 1.2 eV (Figure 1.4b). This value is considerably lower than one reported for typical PAN-derived carbons such as electrospun carbon fibers (FWHM ~ 2 eV) [57] or even for such well-defined systems as g-C_3N_4 (FWHM ~ 1.5–2 eV) [138]. Since the width of the XPS peak reflects the heterogeneity of the chemical environment of any given species [139, 140], the uniquely narrow width observed for porous nanocarbons discussed here is a strong indication of "clean" exposure of N-containing edges on the pore walls. As described in the remaining sections of this article, high performance of such obtained materials as electrodes for supercapacitors and for oxygen reduction reaction, and as CO_2 sorbents, appears to confirm the high (electro)chemical availability of pyridinic nitrogens facilitated by such "clean" exposure.

1.5 Evidence of Enhanced Electrochemical Performance of Nitrogen-Rich Copolymer-Templated Mesoporous Carbons

1.5.1 Supercapacitors

Supercapacitors are an attractive energy storage device owing to their high power density at energy densities far above those of conventional capacitors [100]. Since supercapacitors store the electrical charge primarily in the electrical double layer (EDL) formed at the electrode/electrolyte interface [100], an ideal supercapacitor material should show a combination of high surface area (500–3000 $cm^2\ g^{-1}$) and high accessibility to the pore network.

The importance of high surface area as a factor determining the performance of supercapacitors is illustrated in Figure 1.5, which is a compilation of literature data on specific capacitance (in $F\ g^{-1}$) versus specific surface area (in $m^2\ g^{-1}$) for a wide range of porous

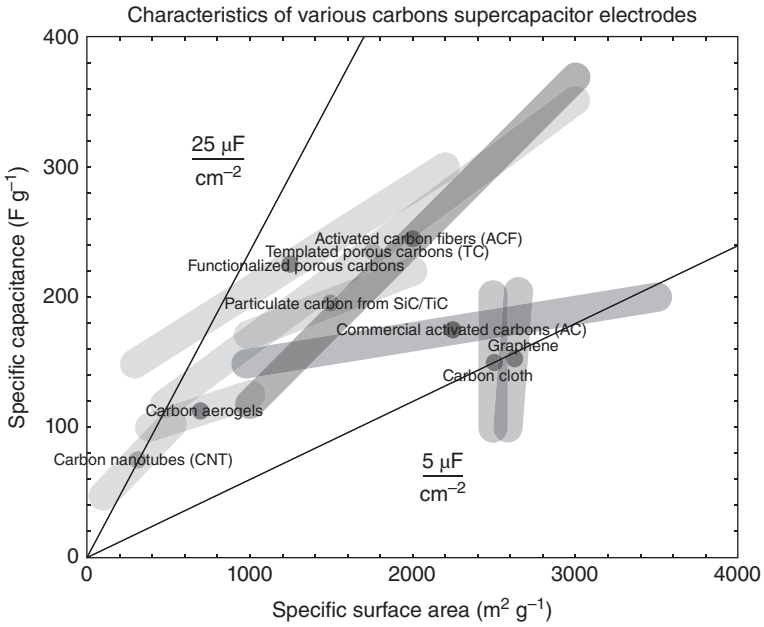

Figure 1.5 Summary plot of specific capacitance and specific surface area values for carbon materials commonly used in supercapacitors. ([8], Reproduced with permission of Wiley.)

carbon materials [141]. While the overall trend of the proportional increase of specific capacitance with the increase of specific surface area is quite clear, the results are broadly distributed, with most of the data points falling within the range of specific capacitances per unit area (C_{sa}) between 5 and 25 μF cm^{-2}, indicated in the plot by two solid lines. Typically, the EDL capacitance is viewed as being limited by the charge density attainable within the double layer, which, in turn depends on physicochemical characteristics of the electrolyte. For common electrolytes, the predicted range of EDL capacitance is between 15 and 25 μF cm^{-2}. Inspection of results summarized in Figure 1.5 shows that a considerable fraction of carbon materials exhibits EDL capacitances well below this range, which suggests that the DOS attainable in the *electrode* rather that within the *electrolyte* is the limiting factor.

There are strong indications that this limitation is related to the orientation of nanographitic domains with respect to pore walls. The primary argument supporting this view comes from the early experiments with electrodes fashioned from blocks of highly ordered pyrolitic graphite (HOPG), which showed a strong dependence of C_{sa} on basal plane orientation with respect to the electrode surface (3 μF cm^{-2} for face-on vs 50 μF cm^{-2} for edge-on orientation) [142]. More recent results with graphene-based supercapacitors, where the basal plane is expected to be a working surface, quote similarly low value of C_{sa} [1]. It should be emphasized that the dependence of C_{sa} on nanographene orientation fits well with the current understanding of the electronic structure of graphene, with edges (in particular zigzag) producing particularly high DOS [27, 31–33].

A widely used approach to increase the energy storage density in materials for supercapacitor electrodes relies on the introduction of an additional charge storage mechanism (pseudocapacitance), involving fast and reversible redox reactions. In carbon materials, this is usually accomplished through the incorporation of heteroatoms such as nitrogen or oxygen within the carbon framework [55, 57, 58, 69, 71, 143]. Pyridinic nitrogen functionalities are particularly sought after as a source of an effective Faradaic process, which involves protonation of the edge pyridinic functionality in acidic electrolyte, as shown in Figure 1.6.

In experiments with supercapacitors, the primary evidence of the benefits of enhanced accessibility of pyridinic nitrogens in CTNCs prepared from AN_{99}-*b*-BA_{70} with bicontinuous morphology comes from the observation that in acidic electrolytes they gave unusually high $C_{sa} = 33\,\mu F\,cm^{-2}$. The pseudocapacitive nature of this enhancement was evident in the characteristically distorted shape of cyclic voltammetry (CV) of carbons pyrolyzed at 700 °C (Figure 1.7a, dots). Consistently with the assignment of the origin of pseudocapacitance to pyridinic nitrogens, no C_{sa} enhancement or CV curve distortion was observed in a basic electrolyte (Figure 1.7a, circles). Further confirmation of the critical role of pyridinic nitrogens came from the CTNCs pyrolyzed at higher temperatures, which, as commonly reported in literature for PAN-derived carbons, exhibited loss of nitrogen content with the increase of pyrolysis temperature. As shown in Figure 1.7b, the C_{sa} for these materials decreased with the pyridinic nitrogen (N-P) content down to the "conventional" level of $\sim 15\,\mu F\,cm^{-2}$, with the shape of CV curve for the material

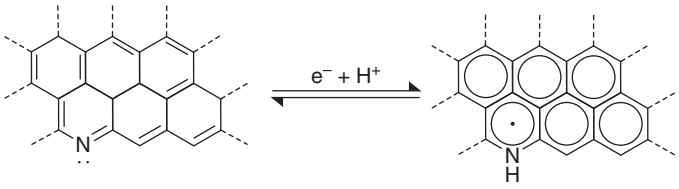

Figure 1.6 Possible pseudo-Faradaic reaction of the pyridinic group in acidic medium [144]. ([8], Reproduced with permission of Wiley.)

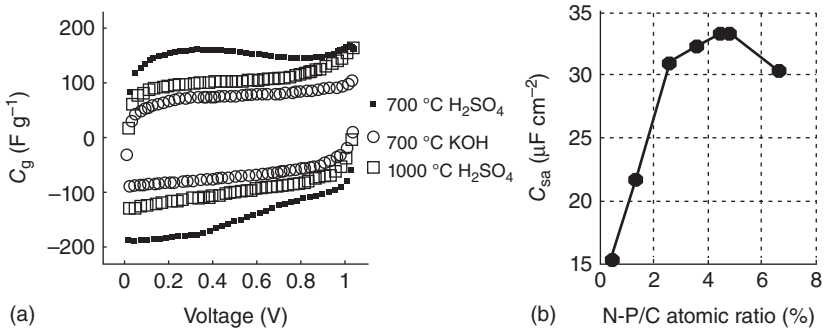

Figure 1.7 (a) Cyclic voltammetry of CTNCs from AN_{99}-*b*-BA_{70} at a scan rate of 2 mV s^{-1} using different pyrolysis temperatures (700 and 1000 °C) and electrolyte (H_2SO_4 and KOH). (b) Specific capacitance plots for CTNCs from AN_{99}-*b*-BA_{70} pyrolyzed at 700 °C in H_2SO_4 electrolyte as a function of pyridinic N-P/C atomic ratio %. ([8], Reproduced with permission of Wiley.)